JACS
JOURNAL OF THE AMERICAN CHEMICAL SOCIETY

Article

pubs.acs.org/JACS

Back Electron–Hole Recombination in Hematite Photoanodes for Water Splitting

Florian Le Formal,*[,†] Stephanie R. Pendlebury,[†] Maurin Cornuz,[‡] S. David Tilley,[‡] Michael Grätzel,[‡] and James R. Durrant*[,†]

[†]Department of Chemistry, Imperial College London, South Kensington Campus, London SW7 2AZ, United Kingdom

[‡]Institut des Sciences et Ingénierie Chimiques, Ecole Polytechnique Fédérale de Lausanne, Laboratory of Photonics and Interfaces, Station 6, CH-1015 Lausanne, Switzerland

Supporting Information

ABSTRACT: The kinetic competition between electron–hole recombination and water oxidation is a key consideration for the development of efficient photoanodes for solar driven water splitting. In this study, we employed three complementary techniques, transient absorption spectroscopy (TAS), transient photocurrent spectroscopy (TPC), and electrochemical impedance spectroscopy (EIS), to address this issue for one of the most widely studied photoanode systems: nanostructured hematite thin films. For the first time, we show a quantitative agreement between all three techniques. In particular, all three methods show the presence of a recombination process on the 10 ms to 1 s time scale, with the time scale and yield of this loss process being dependent upon applied bias. From comparison of data between these techniques, we are able to assign this recombination phase to recombination of bulk hematite electrons with long-lived holes accumulated at the semiconductor/electrolyte interface. The data from all three techniques are shown to be consistent with a simple kinetic model based on competition between this, bias dependent, recombination pathway and water oxidation by these long-lived holes. Contrary to most existing models, this simple model does not require the consideration of surface states located energetically inside the band gap. These data suggest two distinct roles for the space charge layer developed at the semiconductor/electrolyte interface under anodic bias. Under modest anodic bias (just anodic of flatband), this space charge layer enables the spatial separation of initially generated electrons and holes following photon absorption, generating relatively long-lived holes (milliseconds) at the semiconductor surface. However, under such modest bias conditions, the energetic barrier generated by the space charge layer field is insufficient to prevent the subsequent recombination of these holes with electrons in the semiconductor bulk on a time scale faster than water oxidation. Preventing this back electron–hole recombination requires the application of stronger anodic bias, and is a key reason why the onset potential for photocurrent generation in hematite photoanodes is typically ~500 mV anodic of flat band and therefore needs to be accounted for in electrode design for PEC water splitting.

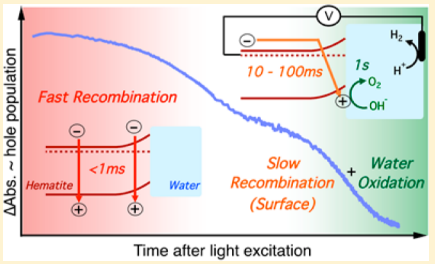

INTRODUCTION

Photoelectrochemical (PEC) solar fuel production, including in particular PEC water splitting, is attracting increased interest, motivated both by recent advances in nanostructured materials and photoelectrochemical interfaces and by concerns over the environmental impact of fossil fuels.[1−4] In such approaches, charge separation across the depletion (or 'space charge') layer formed by the contact of the semiconducting photoelectrode with the electrolyte is a key factor for efficient device function. This charge separation can result (for example for photoanodes) in the accumulation of photogenerated holes at the semiconductor surface with sufficient lifetime to drive water oxidation. The rate constants for water oxidation by such photoaccumulated holes on metal oxide photoanodes have been determined by both optical and electrochemical measurements to be typically in the range 10−0.1 s^{-1}, indicating that such holes must exhibit lifetimes on the order of 0.1−10 s for efficient water oxidation.[5−9] As such, a key issue for this PEC approach is whether the electric field and associated band bending established across the interfacial space charge layer are sufficient to suppress recombination of these accumulated holes with electrons in the bulk of the (typically n-doped) photoanode on this time scale. This recombination loss pathway, which occurs after spatial separation of photogenerated electrons and holes, is potentially in direct kinetic competition with water oxidation by accumulated holes. It has been variously referred to in the literature as 'back electron transfer' or 'surface recombination', with the term 'surface recombination' being typically used to refer specifically to a process occurring via mid-band gap surface states. We will refer herein more generally to the recombination of bulk electrons with holes in the space charge layer as 'back electron–hole recombination'. This recombination is the primary subject of this study.

Received: November 26, 2013
Published: January 17, 2014

   dx.doi.org/10.1021/ja412058x | J. Am. Chem. Soc. 2014, 136, 2564−2574

There is currently significant controversy in the literature over the role of intraband gap surface states in mediating water oxidation by metal oxide photoelectrodes.[6,10] Such surface states have also been suggested to be responsible for surface recombination processes,[11−15] with the passivation of such states being suggested to be a key reason behind the enhancement in device performance often observed following surface treatments.[12,16−18] To a significant extent, this controversy can be attributed to ambiguities in the interpretation or analysis of the different experimental techniques employed to probe these loss processes. In the study reported herein, we employ three complementary techniques, namely, transient absorption spectroscopy (TAS), transient photocurrent measurements (TPC), and electrochemical impedance spectroscopy (EIS), to address the issue of back electron−hole recombination for one of the most widely studied systems, a hematite photoanode. Employing these techniques, we are able to characterize the competition between back electron−hole recombination and water oxidation, and show that all three analysis methods are in quantitative agreement without requiring the inclusion of any intraband gap surface trap states in our analysis.

Due to their high stability and low costs, metal oxide semiconductors are particularly interesting for water splitting devices. Among all oxides, hematite, or α-Fe_2O_3, possesses very promising properties; it is the most stable form of iron oxide at room temperature, and its significant light absorption (band gap of 2.0−2.2 eV) leads to a maximum theoretical Solar-To-Hydrogen (STH) efficiency of 16%.[19] Despite the inadequate position of its band edges and nonideal opto-electronic properties, a hematite-based device including a second photovoltaic cell has recently evidenced unassisted water splitting with an efficiency of 1.2%.[20] Hematite photoanodes with dendritic nanostructure have recently been reported to exhibit photocurrent densities of 3 to 4 mA cm^{-2} at an applied potential of 1.43 V against the reversible hydrogen electrode (RHE).[21,22]

Even with the most successful photoanodes, losses at modest applied potential are significant. This issue is illustrated by the observation that the photocurrent onset potentials for most hematite-based electrodes are reported ∼1.0 V vs RHE as compared to the flat band potential (0.4−0.6 V vs RHE).[19] This requirement for additional voltage to achieve photocurrent generation has been attributed to charge recombination at the semiconductor liquid junction (SCLJ) due to nonideal catalysis or hematite surface defects.[9,23] According to this assignment, surface treatments of hematite with a catalyst (IrO_2, CoPi)[23,24] or with a passivating layer (Al_2O_3, Ga_2O_3)[16,25] have resulted in a cathodic shift of the onset potential.

There is evidence, primarily from transient absorption studies, that rapid (picosecond to millisecond) electron−hole recombination may limit the performance of hematite photoelectrodes,[7,26,27] and that these fast recombination losses may be reduced by the formation of a space charge layer under anodic bias.[7,28] Under these anodic bias conditions, transient absorption studies have provided evidence for the generation of relatively "long-lived" photogenerated holes, which can accumulate at the electrode surface. The lifetime of these "long-lived holes" has been quantified to be ca. 1 s at strong anodic bias, sufficient to promote water oxidation. We have interpreted this observation as indicative of a rate constant for water oxidation by hematite holes of ∼1 s^{-1},[7] consistent with the requirement for a significant accumulation of holes at the hematite surface to generate a high water oxidation photocurrent under steady state irradiation. The amplitude of this long-lived hole signal, measured at 0.1 s, has been correlated with the current density produced by the photoanode.[28] We have also observed an analogous correlation for TiO_2 photoelectrodes.[29] However, such optical studies to date have not explicitly included consideration of back electron−hole recombination on the time scale of water oxidation in the analyses.

A range of photoelectrochemical techniques have also been applied to probe the dynamics of photogenerated hematite holes on millisecond to second time scales. The conclusions of these studies have in some aspects agreed, but in others controversy remains.[6,10−12,30,31] Interfacial, 'surface' or 'back electron transfer' recombination has been identified by several photoelectrochemical methods on the millisecond to second time scale. First, it has been considered to be the origin of the transient currents observed under chopped light illumination.[12,17] Impedance spectra recorded under illumination (Photo-Electrochemical Impedance Spectroscopy or P-EIS) have been reported to demonstrate a second feature at low frequency, which has been assigned to electronic intraband gap surface states promoting charge recombination at the interface.[10] Photogenerated charge recombination on this time scale has also been detected by Intensity Modulated Photocurrent Spectroscopy (IMPS). This loss process was assumed to compete with slow kinetics of water oxidation at small and moderate applied potentials.[6] In some of these studies, intraband gap states are assumed to act as both recombination centers and as charge transfer states mediating water oxidation,[6,10] while in other studies such states only promote surface recombination.[11−13,15] Alternatively, the transient behavior has been described with accumulated positive charges perturbing the space charge layer without invoking their localization in intraband surface states.[32] The disaccord in the models rationalizing the detected processes may be caused, at least in part, by the nontrivial assignment of features in frequency-modulated techniques or by the difficulty of inferring hole dynamics from the monitoring of electron currents. Resolving this ambiguity is essential to design methods reducing back electron−hole recombination and consequently improving photoanodes performance.

Photoanode studies directly comparing hole dynamics determined from transient absorption against those obtained from photoelectrochemical analyses have been very limited to date, complicating comparison of the conclusions determined by these different techniques. In this study, we focus on the role of back electron−hole recombination in limiting the efficiency of hematite photoelectrodes for water oxidation. In particular, we demonstrate a quantitative agreement between three different experimental techniques, transient absorption spectroscopy, transient photocurrent measurements, and electrochemical impedance spectroscopy, on the time scale, bias dependence, and magnitude of this loss pathway. We are thus able to demonstrate that a simple kinetic model based only upon kinetic competition between the reaction of accumulated holes with water (with a bias independent rate constant) and bias dependent back electron−hole recombination is consistent with the data collected by all of these techniques. We furthermore show that all of these kinetic data can be understood without requiring consideration of intraband surface states mediating either recombination or water oxidation processes.

dx.doi.org/10.1021/ja412058x | J. Am. Chem. Soc. 2014, 136, 2564−2574

EXPERIMENTAL SECTION

Hematite Sample. Nanostructured iron oxide samples were prepared by Atmospheric Pressure Chemical Vapor Deposition (APCVD), according to the method developed by Kay et al.[21] and optimized shortly after.[33] The samples investigated in this study are dendritic with 5−10 nm feature size on the top of the nanostructures. The hematite layer is approximately 400 nm thick, doped with silicon (1.5% dopant concentration), and include a SiO_2 buffer layer at the interface with the conductive substrate (FTO TEC15). The role of this underlayer has been discussed previously.[34]

Photoelectrochemical Characterization. Hematite photoanodes were characterized photoelectrochemically in a homemade PTFE cell with quartz windows using an Autolab potentiostat (PGSTAT12) to apply voltage while measuring the current extracted from the sample. A three-electrode configuration was employed, with a Pt gauze counter electrode and a Ag/AgCl/sat. KCl reference electrode. The electrolyte consists of 1 M NaOH (Sigma Aldrich, reagent grade) in Milli-Q-water (Millipore Corp., 18.2 MΩ cm at 25 °C), which gives a pH of 13.6.[35] The sample was irradiated at the electrolyte/semiconductor interface and the illuminated area was determined to be 0.1964 cm^2.

Potentials were applied versus the Ag/AgCl reference electrode (E^0 = +0.197 V vs the standard hydrogen electrode) and are reported against the reversible electrode according to the Nernst equation (eq 1):

$$V_{RHE} = V_{Ag/AgCl} + E^0_{Ag/AgCl} + 0.059\ pH \quad (1)$$

Where V_{RHE} and $V_{Ag/AgCl}$ are the applied potentials against RHE and silver/silver chloride reference electrode, respectively.

Illumination was provided by an array of 12 warm white LEDs (Philips Lumileds, Model white star LXHL-NWE8), placed 12.5 cm in front of the sample. Illumination power was controlled by applying a fixed current to the LEDs. Four different intensities were employed, corresponding to 128.8%, 72.8%, 31.4%, and 15.7% of the AM 1.5 solar spectrum in terms of photon flux below 650 nm as measured with a Silicon photodiode with a short pass filter (650 nm, Edmund Optics).

Transient Absorption Spectroscopy (TAS). Transient optical decays were recorded from the hematite film, using a Nd:YAG laser (Big Sky Laser Technologies Ultra CFR Nd:YAG laser system, 6 ns pulse width). The third harmonic of the laser, corresponding to 355 nm, at a repetition rate of 0.33 Hz, was used as the excitation pulse. A liquid light guide with a diameter of 0.5 cm was used to transmit the laser pulse to the sample. The probe light source was a tungsten lamp (Bentham IL1 tungsten lamp), and the probe wavelength was selected using a monochromator (OBB-2001 dual grating, Photon Technology International) placed prior to the sample. Several long pass and band-pass filters (Comar Instruments) were used to attenuate the laser light arriving at the detector. Transmitted photons were collected with a Si photodiode (Hamamatsu S3071). The detector signal was passed through an amplifier box (Costronics) and recorded using a Tektronics TDS 2012c oscilloscope (microsecond to millisecond time scale) and a National Instruments (NI USB-6211) DAQ card (millisecond to second time scale). The decays presented herein are the average of 200−300 laser pulses. The data were processed using home-built software based on Igor Pro.

The sample was placed in working conditions using the same cell and 3-electrode setup as described in the Photoelectrochemical Characterization section. Potentials were applied between the sample and the reference electrode using a ministat from Sycopel Scientific Ltd.

Electrochemical Impedance Spectroscopy (EIS). Impedance spectra were recorded using the Autolab PG12 apparatus including a Frequency Response Analyzer (FRA) and coupled with Nova electrochemical software. EIS data were gathered using a 10 mV amplitude perturbation between 10 000 and 0.1 Hz, in the dark and under illumination (at the same intensities as mentioned above). The EIS data were simultaneously fit to the equivalent circuits described in the text using Zview software (Scribner Associates).

RESULTS

Sample Photoelectrochemical Performance. Figure 1 shows the current/voltage characteristics of the investigated hematite electrode under dark and different light conditions. Illumination was provided by an array of white LEDs, and was measured to correspond to 16% (blue squares), 31% (green triangles), 73% (orange diamonds) and 129% (red circles) of the photon flux below 650 nm as compared to the AM1.5G solar spectrum. The photoanode performance is consistent with other studies employing this type of nanostructured hematite.[21,36,37] The photocurrent is considered negligible at applied potentials below 0.9−1.0 V_{RHE}, which defines the onset potential. As the applied potential is increased anodically, the photocurrent exhibits a sharp rise and saturates from a potential of ca. 1.3 V_{RHE}. The photocurrent plateau, measured at 1.43 V_{RHE} was found to be linear with the illumination intensity (Figure S1).

The flat band potential has been determined for these nanostructured photoanodes to be between 0.4 and 0.55 V_{RHE} in the same electrolyte.[36,37] Considering the onset potential at 0.9−1.0 V_{RHE} as observed in Figure 1, this demonstrates the typical loss of 0.5 V required for the water splitting reaction to be initiated on hematite electrodes. Previous studies have indicated that applied bias is required to reduce bulk electron−hole recombination (observed on time scales from picoseconds to milliseconds), promoting water oxidation on the surface of hematite.[38] Herein we quantitatively elucidate the effect of recombination at low applied potentials, focusing upon the slow time scale (millisecond to second) dynamics.

Transient Absorption Kinetics. Insight into charge carrier events, including phenomena occurring at the interface with electrolyte, can be gained from transient absorption spectroscopy. A broad transient absorption (TA) signal has previously been assigned to photogenerated holes on visible to NIR wavelengths. To avoid any confusion with another narrower optical feature peaking around 580 nm,[7] the positive charge carriers were characterized by probing the change in absorption at 650 nm.

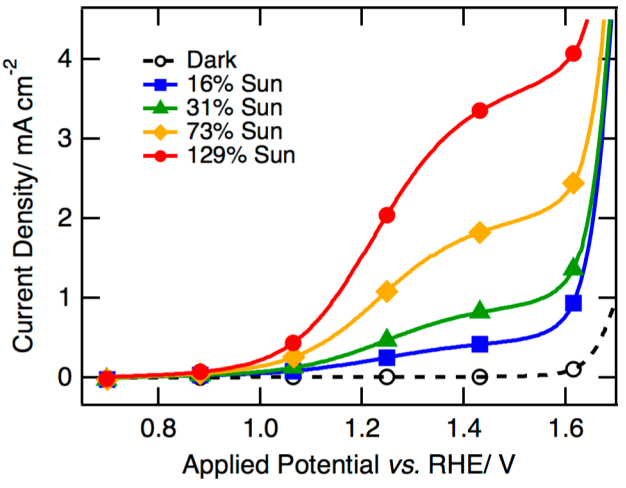

Figure 1. Current densities in mA cm^{-2} of the iron oxide photoanode tested in 1 M NaOH electrolyte, measured in the dark (broken line) and under several illumination intensities (plain lines, see legend for details), are shown as a function of the applied potential, with respect to the reversible hydrogen electrode potential.

dx.doi.org/10.1021/ja412058x | J. Am. Chem. Soc. 2014, 136, 2564−2574

Transient absorption decays measured at this wavelength exhibit two phases, as shown in Figure 2a. To obtain good signal-to-noise ratios, our measurements were spread over several days. To attenuate the effect of the pump intensity variation between measurements, TA signal amplitudes were adjusted to fit the same pattern as the one we previously reported.[28]

The faster decay phase, observed between <1 μs and ca. 20 ms, has been assigned to fast electron−hole recombination. As we have discussed in detail previously, this fast recombination phase is the primary loss pathway limiting the efficiency of electron extraction and hole accumulation at the electrode surface.[7,39] This fast decay is not observed in impedance or photocurrent step analyses, due to these electrons not being extracted and due to slow electron transport kinetics. This fast phase is followed by a slower phase with a lifetime on the milliseconds to seconds time scale, the amplitude of which increases with increasing anodic applied bias. It is this second phase, which we have previously associated with the water oxidation process, which we focus on in this study. In addition to the use of scavengers, one of the key arguments to relate this TA signal to the holes that oxidize water was the appearance of this long-lived signal (second phase) around the onset potential. Accordingly, the amplitude of the TA signal, monitored at 100 ms and 650 nm, has previously been correlated with the photocurrent density associated with water oxidation.[28]

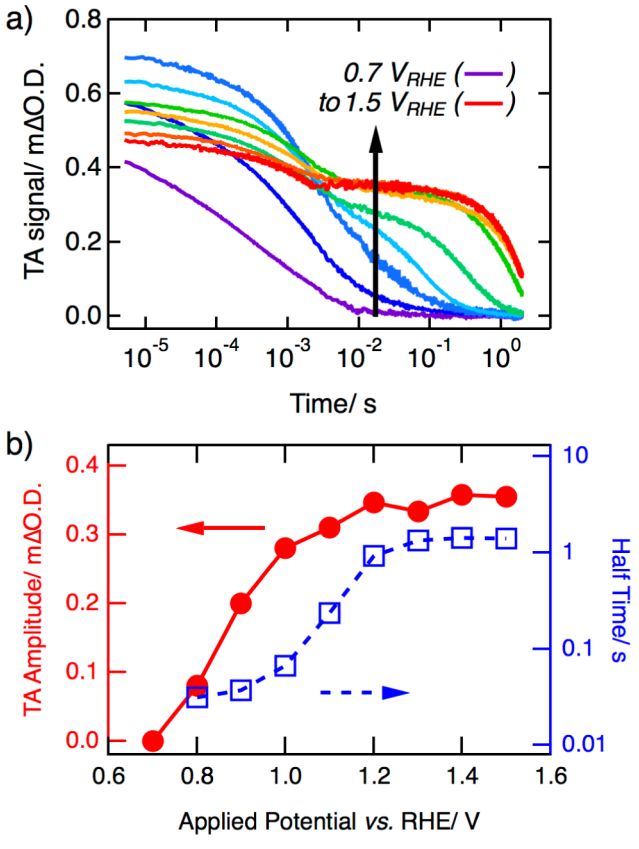

Figure 2. (a) Transient absorption signals for an APCVD hematite film as a function of time after laser perturbation (pumped at 355 nm, probed at 650 nm). The film was held at several different applied potentials during the experiment (in 0.1 V increments; violet, 0.7 V vs RHE; red, 1.5 V vs RHE). (b) Amplitude A_{TA2} (filled red circles, left axis) and half time τ_{TA2} (empty blue square, right axis) of the "long-lived hole" signal monitored at 10 ms are shown against the applied potential with respect to the reversible hydrogen electrode.

Inspection of the data shown in Figure 2 clearly indicates that not only does the amplitude of the second decay phase increase with anodic bias but its lifetime also increases. This trend is also apparent in data reported previously; however, our previous analysis based only on the hole amplitude at 100 ms did not distinguish between this increase in amplitude and in lifetime.[28] Figure 2b shows a plot of the amplitude (A_{TA2}) and halftime (τ_{TA2}) of this slow decay phase determined from a simple biphasic kinetic analysis of the transient decays (full details of the fits, including the fast phase are shown in Supporting Information).

$$\Delta OD(t) = A_{TA1} \exp\left(-\left(\frac{t}{\tau_1}\right)^{\beta_1}\right) + A_{TA2} \exp\left(-\left(\frac{t}{\tau_2}\right)^{\beta_2}\right) \quad (2)$$

It is apparent that the amplitude of this slow phase A_{TA2} increases for biases anodic of 0.8 V_{RHE}, substantially before the onset of photocurrent generation. The initial lifetime of this decay phase also increases with increasing anodic bias from 25 ms to 1.4 s for bias potential ≥1.2 V_{RHE}. This increase in decay half time with anodic bias could originate either from a bias dependence of the water oxidation kinetics or from a bias dependence of an alternative competing pathway such as back electron−hole recombination. To distinguish these two possibilities further, we employed transient photocurrent measurements on the same time scale on the same photoelectrodes, following previous studies which have shown that photocurrent transients can be employed to probe potential back electron−hole recombination (or 'back electron transfer') losses.[12,17]

Photocurrent Transients. Photogenerated electrons were probed by measuring the current flowing between the working electrode and the counter electrode, using the same setup as for TAS. The flow of electrons is shown versus the time after laser excitation for a hematite photoanode held at 0.8 V_{RHE} in Figure 3. The insets to this figure focus on the current measured at long time scales for biases of 0.8 V_{RHE} (blue), 1.0 V_{RHE} (green), 1.2 V_{RHE} (orange) and 1.4 V_{RHE} (red). At short time scales, a large current is extracted from the cell that decays rapidly within the first 10 ms after excitation. After the initial fall off of the positive current, two different behaviors are observed depending on the applied potential. At potentials significantly anodic of flat band (≥1.2 V_{RHE}), the current rapidly stabilizes at a value close to zero. On the other hand, at low applied potentials (0.8 and 1.0 V_{RHE}), the current extracted becomes negative before increasing to reach zero current.

This observation of reverse (negative) electron flow for modest applied potentials indicates that at relatively long times after charge photogeneration, electrons flow from the external circuit back into the hematite photoelectrode. Following previous assignments,[12] this type of behavior is rationalized by considering three successive processes: (i) photogeneration of electrons and holes; (ii) separation of charge carriers, holes reach the surface whereas electrons diffuse to the external circuit; and (iii) holes accumulated at the photoelectrode surface recombine with bulk hematite electrons, inducing a back electron flow from the external circuit into the photoelectrode ('back electron transfer').[40]

The decay times associated with this back flow of electrons can be estimated by determining the half time of the negative

dx.doi.org/10.1021/ja412058x | J. Am. Chem. Soc. 2014, 136, 2564−2574

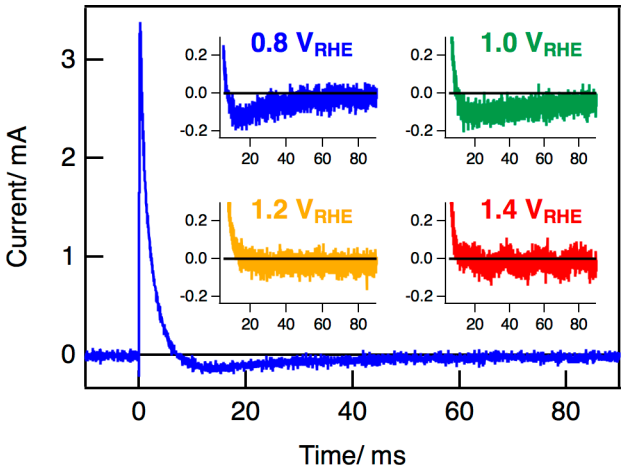

Figure 3. Transient photocurrent measured on the TAS setup at 0.8 V_{RHE} is shown against time after laser excitation (355 nm, 6 ns pulse). Insets show the same type of photocurrents measured when the sample is held at key applied potentials (0.8 V_{RHE}, blue; 1.0 V_{RHE}, green; 1.2 V_{RHE}, yellow; and 1.4 V_{RHE}, red) with focus on the long time scale. It highlights the negative electron flow at small applied potentials by expanding the current measured in the 10 ms to 100 ms time scale.

current transients. Half times of 20 and 80 ms are obtained when the sample is held at 0.8 and 1.0 V_{RHE}, respectively. It thus appears that charge recombination due to the back electron transfer flow in these electrodes occurs in the same time range at which long-lived holes are observed in the transient absorption data (10 ms to 1 s), and must therefore be considered in analyses of these transient absorption data.

Kinetic Competition between Water Oxidation and Back Electron Recombination. On the basis of the transient absorption and photocurrent data reported above, we now consider a simple kinetic model to describe the kinetic competition between water oxidation and the recombination related to the electron back flow (back electron recombination). In this model, the decay rate constant of the long-lived hole signal observed in our transient absorption data (k_{TA2}, corresponding to ln 2 × τ_{TA2}^{-1}, see Figure 2b) is equal to the sum of the rate constants representing the two competing processes, as described by eq 3.

$$k_{TA2}\,(V) = k_{WO} + k_{BER}\,(V) = \ln 2 \times (\tau_{TA2})^{-1} \qquad (3)$$

where k_{WO} is the apparent rate constant for water oxidation,[41] and k_{BER} is the rate constant for back electron recombination. k_{WO} is assumed to be independent of the applied potential, consistent with our previous observations,[5] and equal to the long-lived hole decay rate constant at high applied bias (1.5 V_{RHE}), where back electron–hole recombination is assumed to be negligible compared to water oxidation. This yields a rate constant of 0.7 s^{-1} for water oxidation, which agrees with the range previously reported for this process from TAS and photoelectrochemical studies (0.3–1 s^{-1}).[7,42] k_{BER} is calculated according to eq 3, and is allowed to be bias dependent, consistent with previous literature.[6] This model is in agreement with that previously employed by Peter[17] to analyze EIS and IMPS data, except that for simplicity we have not included a bias dependent water oxidation rate constant.

The rate constants from analyzing the transient absorption data according to this simple kinetic model are shown against the applied potential in Figure 4a. Also shown are the rate

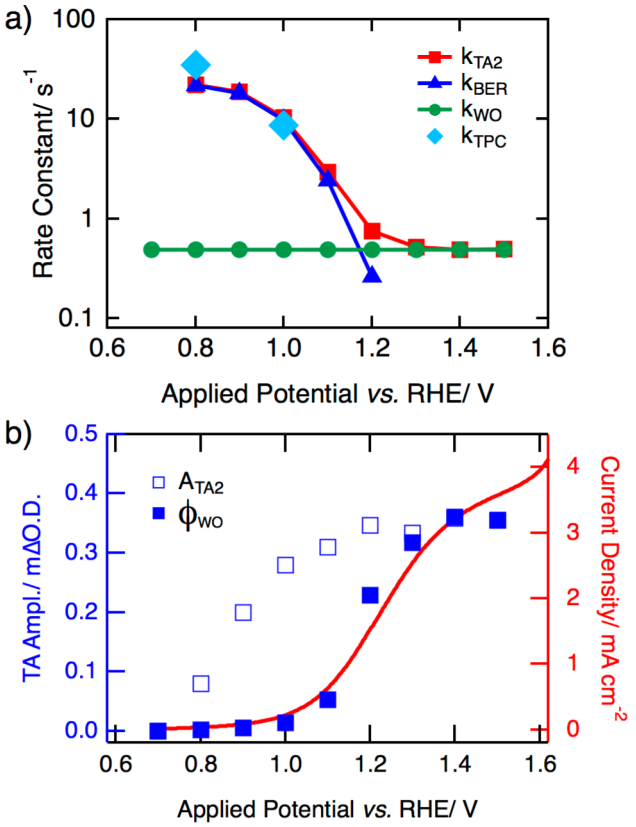

Figure 4. (a) Rate constants extracted from TPC (light blue diamonds) and TA spectroscopy (red squares for k_{TA2}, dark blue triangles for k_{BER}, green circles for k_{WO}) are shown as a function of the applied potential, with respect to the reversible hydrogen potential. (b) Comparison between the TA signal amplitude A_{TA2} obtained from fitting (empty blue squares, left axis), corresponding to the yield of long-lived holes, and the water oxidation yield ϕ_{WO} determined from the TA data by eq 4 assigned to water oxidation (full blue squares, left axis) versus the photocurrent measured at 1.3 sun (red trace, right axis) at different applied potentials.

constants for back electron transfer from the photocurrent transients. At low applied potentials (0.8–1 V_{RHE}), back electron recombination appears to be the dominant decay process, with the decay time of photogenerated holes observed in the transient absorption data being in excellent quantitative agreement with the decay times of the negative photocurrent transients. In contrast, at high potentials (≥1.4 V_{RHE}), the decay of the long-lived hole signal is associated primarily with water oxidation. Competition between the two processes is apparent between 1.0 and 1.3 V_{RHE}, corresponding to applied potentials where the photocurrent density exhibits a sharp increase (Figure 1).

Following this simple kinetic model, the quantum yield of holes achieving water oxidation (ϕ_{WO}) is given by:

$$\phi_{WO} = A_{TA2} \times \frac{k_{WO}}{k_{TA2}} \qquad (4)$$

where A_{TA2} is the initial amplitude of the second hole decay phase observed in the transient absorption data (see Figure 2b). This amplitude assays the yield of long-lived holes accumulating at the photoelectrode surface. The proportion of these long-lived holes reacting with water is represented by the ratio of rate constants k_{WO}/k_{TA2}.

dx.doi.org/10.1021/ja412058x | J. Am. Chem. Soc. 2014, 136, 2564–2574

In Figure 4b, we plot the dependencies of ϕ_{WO} and A_{TA2} versus applied bias and compare these to the bias dependence of photocurrent density. It is apparent that there is an excellent correlation between the yield, ϕ_{WO}, of holes achieving water oxidation determined from our simple kinetic analysis of the transient absorption data and the observed photocurrent density. Similar to the photocurrent, ϕ_{WO} is negligible until 1.0 V_{RHE}, then rises sharply with increasing potential and saturates at ca. 1.3 V_{RHE}. On the contrary, the initial yield of long-lived holes rises from 0.8 V_{RHE}, significantly cathodic of the onset of photocurrent generation. This latter type of behavior with applied potential is analogous to the instantaneous amplitude of the transient photocurrent studies with light on/off steps.[12]

These results indicate that the TA second phase is associated with the combination of two slow processes, i.e., recombination and water oxidation. The kinetic model employed is beneficial to distinguish holes recombining and holes reacting with water (related to the steady state photocurrent). This highlights the losses at long time scales occurring at low bias potential due to the back electron current.

Impedance Spectroscopy. (Photo-)Electrochemical Impedance Spectroscopy (EIS or PEIS) is another widely used electrochemical technique, which can provide insight into electronic behavior during water splitting. Briefly, it consists of measuring the complex current response of a photoanode to a frequency modulated voltage perturbation. Under dark conditions, hematite photoanodes typically only exhibit a single feature in EIS analyses; the associated capacitance is assigned to the space charge layer. Of particular interest for the photoelectrochemical function of these photoanodes, an additional feature at low frequencies (a second semicircle in a Nyquist plot) is observed under irradiation. We focus herein on the behavior and assignment of this second, light induced, feature.

To analyze the data acquired under different illumination intensities, we use two equivalent circuits (Figure 5 a,b), which are simplifications of a more general model recently proposed to describe hematite photoanode behavior.[10] The circuit elements related to the second feature observable under illumination are R_{light}, C_{light} and (for Model b only) $R_{CT\text{-}light}$. Assignment of these features is examined in the Discussion section below. Complete analysis of the P-EIS signature of APCVD hematite photoanodes is beyond the scope of this article but some of the main features are presented below.

The capacitance C_{light} obtained from fitting the impedance data with equivalent circuits (a) (plain lines and full circles) and (b) (broken lines and empty circles) is shown in Figure 5c. In both cases, the capacitance is negligible at low applied potentials, and peaks at potentials anodic of the onset potential before decreasing at high potentials. Moreover, fitting results from the two equivalent circuits exhibit the same trend: the capacitance amplitude increases and shifts anodically with increasing bias light intensity. The potential where C_{light} is maximum varies from about 1.1 to 1.2 V_{RHE} for model (a) to 1.25−1.3 V_{RHE} for model (b).

The second process, only induced under illumination, can be characterized with the rate constant related to the charging or discharging of C_{light}, independent of which equivalent circuit is used to model the impedance response. This corresponds to the inverse of the RC time constant obtained by multiplying the value of C_{light} with the equivalent resistance through which charges are extracted (see Supporting Information for full analysis). As shown in Figure 5d, the rate constant assigned to C_{light} charging/discharging is in the 100−1 s^{-1} range. Similarly with the other techniques discussed above, this process associated with photogenerated charges slows down with increasing positive applied potential. Additionally, this process is faster (higher rate constant) with higher illumination, suggesting that the kinetics involved are dependent on the number of photogenerated charges (the number of photogenerated charges being proportional to the illumination

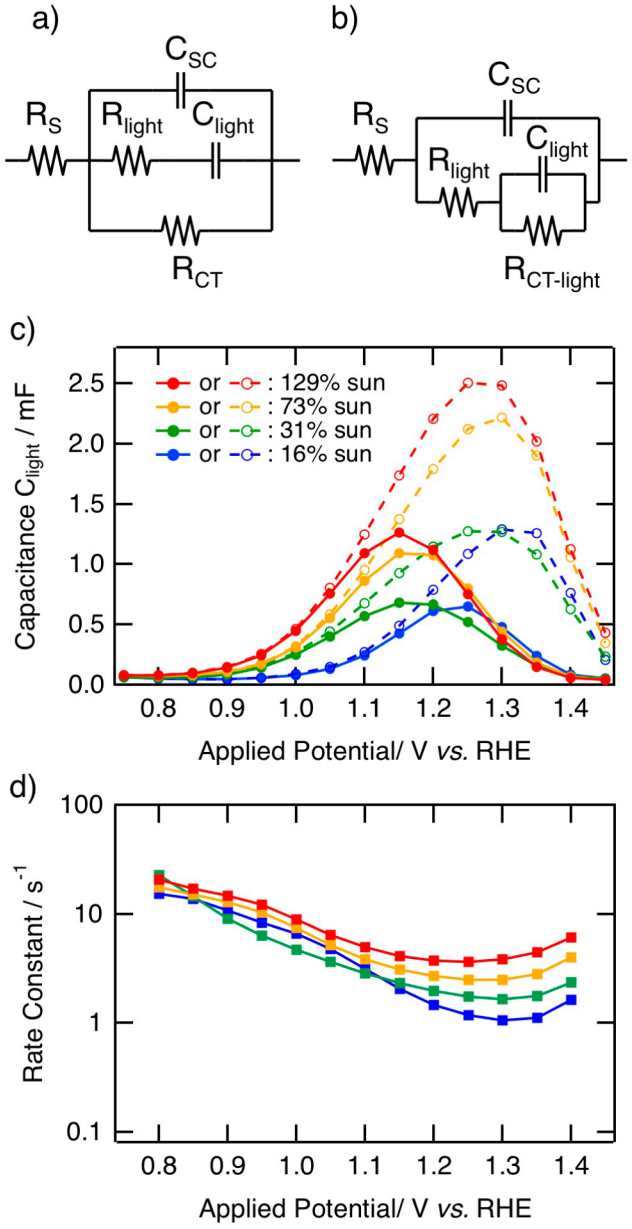

Figure 5. (a and b) Equivalent circuits used to fit the EIS response of a hematite photoanode under illumination. These models are simplifications of the model presented in ref 3. All notations are explained in the text. (c) Fitted capacitance C_{light} is shown at several bias light intensities (see legend) against the applied bias potential vs RHE, from the data fitted with model a (full circles and plain lines) and with model b (empty circles and broken lines). (d) Rate constants related to the charging/discharging of C_{light} is shown for model a at several bias light intensities (same as (b)), against applied potential vs RHE. Fitting with model b results in the same values of the rate constant.

dx.doi.org/10.1021/ja412058x | J. Am. Chem. Soc. 2014, 136, 2564−2574

intensity). We would like to emphasize that the characterization of this process is not model-dependent, as the same rate constant is obtained for equivalent circuits (a) and (b).

Comparison between Techniques. From visual comparison of Figures 4a and 5d, it is apparent that the time scale and the bias dependence of the processes elucidated by all three techniques are similar. The comparison between the recombination processes elucidated by the different techniques used in this study is shown in Figure 6, in terms of rate constant (Figure 6a) and amplitude (Figure 6b). Also overlaid are the characteristics of the recombination process (rate constant and amplitude) determined previously from analyses of photocurrent transients for analogous hematite films from light on/off step studies (see description below).[12]

In Figure 6a, the bias dependence of the surface recombination rate constant determined from the TPC transients (light blue squares) and analyses of the transient absorption data (red diamonds, as shown in Figure 4a) is compared with the rate constants obtained from EIS analysis (violet triangles, also shown in Figure 5b) and for the decay of accumulated holes defined in previous transient photocurrent studies (orange squares). It is apparent that all four techniques give similar rate constants and bias dependencies, particularly for more modest applied bias.

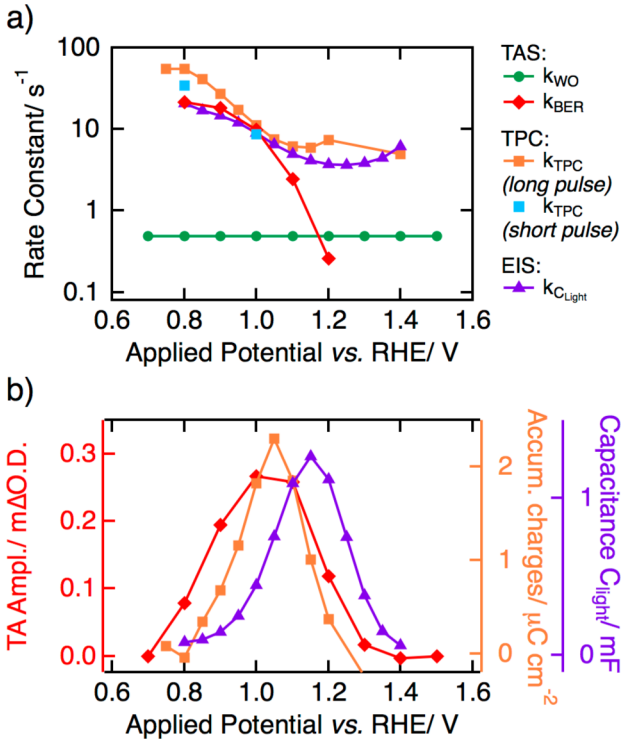

Figure 6. Comparison of the back electron recombination process evidenced by optical and photoelectrochemical techniques in terms of rate constant (a) and amplitudes (b). (a) Rate constants obtained for water oxidation (k_{WO} from TAS, green circles), and for back electron–hole recombination obtained from TAS (k_{BER}, red diamonds, under pulsed 200 μJ cm^{-2} monochromatic illumination), short pulse TPC (light blue squares, same illumination as TAS), long pulse TPC (orange squares, 1 sun bias light, adapted from ref 8) and EIS (violet triangles, 1.3 sun bias light) are shown against the applied potential, with respect to the RHE. (b) Amplitudes of the TA signal assigned to holes inducing back electron–hole recombination (red diamonds, left axis), the capacitance C_{light} extracted from EIS and assigned to the back electron–hole recombination (violet triangles, violet right axis) and the hole density involved in back electron–hole recombination during long pulse TPC experiments (orange squares, orange right axis, adapted from ref 8) are shown against the applied potential with respect to RHE.

Amplitudes of the recombination signal elucidated by transient absorption, EIS analysis and transient photocurrent (with light on/off steps) are compared in Figure 6b. The amplitude of the recombination signal has been obtained by quantifying the TA signal assigned to holes recombining (eq 5), in similarity to the calculation of the quantity of holes reacting with water (eq 4).

$$\phi_{BER} = A_{TA2} \times \frac{k_{BER}}{k_{TA2}} \quad (5)$$

This amplitude ϕ_{BER} is equivalent to the proportion of photogenerated holes recombining by back electron–hole recombination determined from the investigation of transient photocurrents.[12] It is particularly noticeable that both techniques indicate this loss pathway peaks at the same applied potential, which also corresponds to the onset of the steady state photocurrent. However, the maximum of the capacitance C_{light} obtained from EIS analysis (model a) is anodically shifted as compared to the onset potential. This can be explained by the probe species perceived by the different experiment techniques. The two first techniques are assumed to monitor charges (holes here) whereas impedance spectroscopy detects variation of electron currents. If the capacitance related to this variation of current is nonlinear with the applied voltage, then it is defined by the differential of the stored charges over the voltage causing the field (C = dQ/dV). In this case, the capacitance peaks at the voltage where the slope defined by Q vs V is maximum. From visual inspection of Figure 6b and accounting for the negative charge of the electron, the maximum of the capacitance C_{light} (taken from fitting with model 5a) correlates adequately with the maximum in slope of the hole density vs voltage characteristics, demonstrated by the two other experiments. We also note that this difference may be related to the transient absorption data employing pulsed optical excitation, while the impedance data employs continuous irradiation; transient absorption studies under both pulsed and continuous irradiation are ongoing and will be reported elsewhere.

DISCUSSION

Assignment of Back Electron Current/Recombination. Transient absorption (TA) studies indicate that the decay half time of the slow decay phase assigned to long-lived holes accumulated at the hematite surface increases with anodic bias. This bias dependence is analyzed in terms of a simple model between bias independent water oxidation and bias dependent back electron–hole recombination. The rate constant for this recombination reaction and its bias dependence is shown to be in quantitative agreement with data obtained from transient photocurrent (TPC) and electrochemical impedance (EIS) analyses. The negative current detected by TPC indicates that electrons flow back toward the surface of hematite with a ca. 100–1 s^{-1} rate constant. EIS performed under illumination provides evidence for capacitive behavior, with charging and discharging being characterized with a rate constant between 100 and 1 s^{-1}.

These observations agree with previous studies of charge accumulation by transient photocurrent spectroscopy, when

dx.doi.org/10.1021/ja412058x | J. Am. Chem. Soc. 2014, 136, 2564–2574

illuminating the sample on a time length sufficient for the photocurrent to stabilize at each step.[12] The anodic photocurrent peak when light is switched on and the cathodic peak when illumination is stopped have been rationalized in terms of accumulated charges and back electron flow. During the light pulse, holes accumulated in proximity to the SCLJ are assumed to perturb the space charge layer (and its electric field)[32] and/or to cause the establishment of an electron flow toward the surface.[6] The electrons diffusing from the external circuit recombine with accumulated holes at the interface. Eventually equilibrium is reached between the density of holes accumulated causing the back electron flow and the density of holes recombining. This results in an apparent constant amount of accumulated positive charge at the surface. After the light pulse, the electron back flow persists up to the time when the material surface recovers its steady state prelight pulse.

The experiments (from which the rate constants and amplitudes shown in Figure 6) were performed holding the hematite photoanode at a fixed bias potential and illumination (1 sun), and applying a light pulse of 0.5 s from a blue LED. The rate constant obtained for the decay of negative current after illumination is shown in Figure 6a. It is worth noting here that a similar rate constant is obtained for the photocurrent decay during the light pulse, indicating that the two phenomena are related to the same process (Figure S4 in Supporting Information). The rate constant for this process is consistent with the others measured in our study.

The rate constant for the back electron−hole recombination process characterized by intensity modulated photocurrent spectroscopy (IMPS) is also in agreement with our results. Surface losses have been characterized with a rate constant between 100 and 1 s^{-1} when the applied potential was set between 0.8 and 1.6 V_{RHE}.[6]

The combination of all these techniques allows the assignment of the investigated process. Our results strongly indicate that all the characterization techniques discussed herein describe the same recombination phenomenon with a rate constant of 100−1 s^{-1} for hematite photoanodes held at low applied potentials. This process is assigned to back electron flow initiated by accumulated charges on the surface of the electrode and resulting in surface recombination. This assignment does not require considering the accumulation of positive charges in intraband gap trap states but is based on the low water oxidation rate constant. This slow process allows the establishment of a positive charge at the interface, building an electron back current when the space charge depth and field are not large enough to repulse electrons.

Consequently, the circuit elements related to the feature observable under illumination in impedance spectra (see Figure 5a,b) are assigned to the electron back flow initiated during illumination by the accumulation of positive charge at the interface. C_{light} is assigned to the capacitance of the constant density of holes accumulated at the SCLJ that induce interfacial recombination. From our results, the model (a) (Figure 5) better fits the characteristic of the recombination process obtained by other techniques, especially in terms of amplitude maximum. This model differentiates the paths (resistances) for the two types of current, i.e., the electron current due to hole consumption at the interface (water oxidation) and the back electron flow, even if the holes reacting and the ones recombining are not differentiated.

Effect of Illumination on the Recombination Process. The kinetics of the recombination process detected by EIS have been shown to depend on the intensity of the bias light (Figure 5c). This is in agreement with another impedance study where the recombination rate constant increased with decreasing bias light intensity.[42] Consequently, the small deviation observed between rate constants in Figure 6 can be explained by the different illumination intensities used: TAS and short pulse TPC were measured with continuous 650 nm illumination (probe) and a 200 μJ cm^{-2} pulsed monochromatic light perturbation (355 nm), while the EIS rate constant corresponds to continuous 129% AM1.5 illumination.

The capacitance C_{light} also increases with the illumination intensity (Figure 5b), implying a greater number of accumulated charges inducing the back electron current. Therefore, increasing the illumination intensity results in a higher density of accumulated charges, which more significantly perturb the space charge layer. The surface recombination process appears to be faster with an increased number of accumulated charges under more intense illumination.

Recombination at Small Bias Potential. We have recently observed a correlation between the TA signal amplitude of long-lived holes with the depletion layer width in undoped $BiVO_4$ photoanodes, another promising system for water splitting (unpublished data). In hematite, however, the long-lived hole signal amplitude, measured at 10 ms, does not correlate with the space charge layer width, calculated with a donor density of 10^{20} cm^{-3} and a flat band potential of 0.55 V_{RHE} (see Figure S5 in Supporting Information). This discrepancy in behavior is also evidenced by the observation that below 0.75 V_{RHE} (equivalent to 0.2−0.25 V anodic of the flat band potential), neither charge accumulation nor surface recombination is detected in hematite.

At any applied potential greater than 0.7 V_{RHE}, the TA decay is composed of two phases: one fast with a decay half time below 10 ms and one slower with a decay half time increasing from 10 ms to 1s with applied potential (see Figure 2a). The fast phase, assigned primarily to recombination of charges not sufficiently separated, is also evidenced at very small potentials (between flat band and 0.8 V_{RHE})[28] and has been shown to be slowed down with increasing applied bias potential. This retardation of the fast recombination losses is initiated as soon as applied bias is positive of flat band. This indicates that at small applied potentials, charges are photogenerated in the depletion layer but the field is not large enough to enable sufficient spatial separation of electrons and holes. Additionally, localized electronic states, located just below or at the bottom of the conduction band, could function as trapping/recombination sites for charges inside the depletion layer. Such states have been associated with a negative signal (corresponding to a bleach, a loss of absorption) detected in hematite samples while probing TA at 580 nm.[7] The amplitude of this negative feature (observed before 10 ms) has been shown to increase with applied potential similarly to the depletion layer thickness (i.e., following a square root law). This correlation suggests that electrons photogenerated in the space charge layer thermalize to these electronic states before they either recombine or diffuse to the external circuit. The presence of such localized electronic states may favor the recombination observed before 1 ms, which occurs at applied potentials between flat band and the onset of the long-lived hole signal. This recombination process, through the space charge layer or mediated by trap states localized below the conduction band, limits the generation of long-lived holes.

dx.doi.org/10.1021/ja412058x | J. Am. Chem. Soc. 2014, 136, 2564−2574

At modest anodic potentials, the retardation of the recombination phase is sufficient to observe the accumulation of long-lived holes at the interface. These accumulated holes can induce a back electron current or react with water (at bias potentials anodic of the photocurrent onset). These two latter processes are competing at bias potentials between 0.8 and 1.3 V_{RHE}.

Disappearance of the Recombination Signal at High Bias Potential. Our results suggest that back electron−hole recombination does not occur when the hematite photoanode is held at a bias potential greater than 1.2−1.3 V_{RHE}.

Two explanations have been proposed in the literature for the reduction in the amplitude of the EIS and photocurrent transients at high applied biases. First, charge accumulation has been assumed to occur in trap states, localized energetically at ca. 0.5 V below the conduction band. This is supported by the observation of two different types of holes in soft X-ray spectroscopy,[30] by sub-band gap absorption[32] and by photopotential studies.[43,44] These trap states, assumed to be iron atoms in high valence states,[42] have been considered to act as recombination centers and sometimes as the preferred pathway for water oxidation. These surface states are potentially inactivated when the Fermi level is set below these states, i.e., when they are not occupied by electrons. Additionally, surface states have been supposed to be deactivated by coating the surface of the hematite photoanode with alumina or with a cobalt-based layer.[12] The lower charge accumulation and the lower potential where the density of accumulated charges peaks observed have been related to the cathodic shift of the water oxidation photocurrent. A second reason considered for the disappearance of charge recombination at high potential is the acceleration of the hole transfer rate with increasing bias. The bias dependent rate constants for water oxidation and recombination, characterized with IMPS, have been evidenced to cross at ca. 1.2−1.3 V_{RHE}.[6] Thus, surface recombination is prevented when the rate constant associated with surface recombination becomes shorter than the one related to water oxidation.

The data we report herein suggests an alternative explanation for the prevention of slow recombination losses at large anodic potentials. The increase in applied bias potential enhances both the width of the depletion layer and its related field. At moderate applied potentials (0.8−1.3 V_{RHE}), the space charge field can separate the photogenerated charges but is not large enough to block the back flow of electrons induced by accumulated holes at the interface. Yet at large potentials, over 1.3 V_{RHE} (0.8 V vs flat band), the space charge width and field are large enough to repulse electrons and inhibit this recombination path. This explanation is broadly consistent with that proposed in reference 17.

We note that the model we propose does not imply the absence of intraband gap states at the hematite surface. Indeed there is extensive evidence for the presence of such states, and their modulation by surface treatments.[17,25,45,46] It only indicates that the photoelectrochemical function of the hematite photoanodes studied herein can be understood without explicit consideration of these states being directly involved in the recombination and water oxidation pathways of these electrodes.

Our interpretation implies that the space charge layer has two distinct roles in inhibiting electron−hole recombination, operating on two very different time scales. First, the space charge layer needs to be large enough to retard the fast recombination (<10 ms), leading to spatial separation of electrons and holes and the accumulation of long-lived holes at the electrode surface. Second, the space charge layer (and its related field) needs to be increased significantly more to stop the back electron flow (10 ms to 10 s) induced by the accumulated holes. Both recombination processes involve the recombination of hematite electrons and holes; they are however distinct as the latter process requires a thermal activation or tunneling across the space charge layer, and therefore occurs on much slower time scales, and with a different dependence on applied bias.

Implication of Back Electron Flow for PEC Design. The results presented in this study underline the significant losses occurring at low and moderate bias potential due to the back electron flow induced by hole accumulation at the interface. Therefore, this recombination process has to be taken into account in the design of PEC electrodes. It appears to be reduced when the hematite sample is held at large anodic potential, i.e., when the space charge layer thickness and its associated field are significant. A thicker depletion layer at small applied potentials can be obtained if the hematite donor density is reduced by, for example, decreasing the dopant concentration. However, the addition of dopants has been previously shown to induce favorable electronic and structural changes in hematite.[47] The drop in electronic conductivity could be overcome by using a host−guest approach, where a thin layer of hematite completes light absorption and surface reaction whereas the electron collection is achieved by another material.[48,49]

A second path for improvement is the addition of overlayers on the surface of the hematite photoanode. Surface coating with inorganic layers (Ga_2O_3, Al_2O_3)[16,25] has been shown to decrease the surface hole accumulation at low bias, cathodically shifting the onset of the photocurrent. This effect has been rationalized by the passivation of surface states and by the increased electron repulsion from the surface.[12] The latter process, involving an electron rich layer on the surface, can also be invoked without considering surface states. Surface coverage with catalysts (IrO_2, CoPi)[23,24] has also resulted in a cathodic shift in photocurrent onset, which has been attributed to an increased distance between the electrons at the edge of the depletion layer and holes extracted to the catalyst layer.[12] Finally, it was also suggested that surface treatments, including both Ga_2O_3 and CoPi overlayers, can result in increased space charge layer formation, and therefore reduced recombination losses.[18] Interestingly, the effects of inorganic layers and catalyst layers can be combined to further decrease the onset potential.

■ CONCLUSION

Transient absorption spectroscopy was employed to characterize the processes involving photogenerated holes in hematite photoanodes. The previous assignment of the bias-dependent second phase in TA spectra, from 1 ms after excitation to long-lived holes performing water splitting, was improved. This was achieved by considering a back electron current inducing recombination with "long-lived holes" at the interface and competing with water oxidation on longer time scales. The corrected signal assigned to holes reacting with water was found to better correlate with photocurrent extracted from the film. Additionally, two rate constants were extracted from this study: one at ca. 0.5 s^{-1}, assigned to water oxidation and assumed constant with bias potential, and the other in the 100−1 s^{-1} range, related to back electron recombination.

This latter rate constant was compared to other processes observed in transient photocurrent (TPC) measurements and photoelectrochemical impedance spectroscopy (PEIS). We found a good agreement between all three techniques characterizing the losses at the semiconductor-liquid interface.

This study highlights the significance of a back electron−hole recombination loss process on the surface of water splitting photoanodes, retarding the appearance of the photocurrent and requiring a greater amount of energy from a second solar device. The comparison between several techniques confirms that a similar phenomenon is described by all of types of measurement employed. Further studies will focus on illumination intensity effects and on surface treatments that have shown a cathodic shift in the photocurrent onset. This type of treatment, as well as better understanding of the behavior of electronic charges on the surface of metal oxide semiconductors, is of great importance for the use of this inexpensive type of material in opto-electronic devices.

■ ASSOCIATED CONTENT

Ⓢ Supporting Information

Linearity of photocurrent with illumination power, parameters obtained from the fit of TA decays, analysis of equivalent resistances in EIS equivalent circuits, time constants related to processes detected by on/off step illumination and comparison between the TA signal and the space charge width. This material is available free of charge via the Internet at http://pubs.acs.org.

■ AUTHOR INFORMATION

Corresponding Authors

f.le-formal@imperial.ac.uk
j.durrant@imperial.ac.uk

Notes

The authors declare no competing financial interest.

■ ACKNOWLEDGMENTS

F.L.F., S.R.P. and J.R.D. thank the European Science Foundation (project Intersolar 291482) for funding. F.L.F. thanks the Swiss National science Foundation (project: 140709). M.C., S.D.T., and M.G. thank the Swiss Federal Office for Energy (PECHouse Competence Center, contract number SI/500090−02). The authors also thank Dr. Piers Barnes for fruitful discussions.

■ REFERENCES

(1) Grätzel, M. *Nature* **2001**, *414*, 338−344.
(2) Walter, M. G.; Warren, E. L.; McKone, J. R.; Boettcher, S. W.; Mi, Q.; Santori, E. A.; Lewis, N. S. *Chem. Rev.* **2010**, *110*, 6446−6473.
(3) Osterloh, F. E. *Chem. Soc. Rev.* **2013**, *42*, 2294−2320.
(4) Cowan, A. J.; Durrant, J. R. *Chem. Soc. Rev.* **2013**, *42*, 2281−2293.
(5) Cowan, A. J.; Barnett, C. J.; Pendlebury, S. R.; Barroso, M.; Sivula, K.; Grätzel, M.; Durrant, J. R.; Klug, D. R. *J. Am. Chem. Soc.* **2011**, *133*, 10134−10140.
(6) Peter, L. M.; Wijayantha, K. G. U.; Tahir, A. A. *Faraday Discuss.* **2012**, *155*, 309−322.
(7) Barroso, M.; Pendlebury, S. R.; Cowan, A. J.; Durrant, J. R. *Chem. Sci.* **2013**, *4*, 2724−2734.
(8) Pesci, F. M.; Cowan, A. J.; Alexander, B. D.; Durrant, J. R.; Klug, D. R. *J. Phys. Chem. Lett.* **2011**, *2*, 1900−1903.
(9) Dare-Edwards, M.; Goodenough, J.; Hamnett, A.; Trevellick, P. *J. Chem. Soc., Faraday Trans. 1* **1983**, *79*, 2027−2041.
(10) Klahr, B.; Gimenez, S.; Fabregat-Santiago, F.; Hamann, T.; Bisquert, J. *J. Am. Chem. Soc.* **2012**, *134*, 4294−4302.
(11) Glasscock, J. A.; Barnes, P. R. F.; Plumb, I. C.; Savvides, N. *J. Phys. Chem. C* **2007**, *111*, 16477−16488.
(12) Le Formal, F.; Sivula, K.; Grätzel, M. *J. Phys. Chem. C* **2012**, *116*, 26707−26720.
(13) Ahmed, S.; Leduc, J.; Haller, S. *J. Phys. Chem.* **1988**, *92*, 6655−6660.
(14) Iwanski, P.; Curran, J.; Gissler, W.; Memming, R. *J. Electrochem. Soc.* **1981**, *128*, 2128−2133.
(15) Horowitz, G. *J. Electroanal. Chem.* **1983**, *159*, 421−436.
(16) Hisatomi, T.; Le Formal, F.; Cornuz, M.; Brillet, J.; Tetreault, N.; Sivula, K.; Grätzel, M. *Energy Environ. Sci.* **2011**, *4*, 2512−2515.
(17) Peter, L. M. *J Solid State Electrochem.* **2013**, *17*, 315−326.
(18) Barroso, M.; Mesa, C. A.; Pendlebury, S. R.; Cowan, A. J.; Hisatomi, T.; Sivula, K.; Grätzel, M.; Klug, D. R.; Durrant, J. R. *Proc. Natl. Acad. Sci. U.S.A.* **2012**, *109*, 15640−15645.
(19) Sivula, K.; Le Formal, F.; Grätzel, M. *ChemSusChem* **2011**, *4*, 432−449.
(20) Brillet, J.; Yum, J.-H.; Cornuz, M.; Hisatomi, T.; Solarska, R.; Augustynski, J.; Grätzel, M.; Sivula, K. *Nat. Photonics* **2012**, *6*, 824−828.
(21) Kay, A.; Cesar, I.; Grätzel, M. *J. Am. Chem. Soc.* **2006**, *128*, 15714−15721.
(22) Warren, S. C.; Voïtchovsky, K.; Dotan, H.; Leroy, C. M.; Cornuz, M.; Stellacci, F.; Hébert, C.; Rothschild, A.; Grätzel, M. *Nat. Mater.* **2013**, *12*, 842−849.
(23) Tilley, S. D.; Cornuz, M.; Sivula, K.; Grätzel, M. *Angew. Chem., Int. Ed.* **2010**, *49*, 6405−6408.
(24) Zhong, D. K.; Cornuz, M.; Sivula, K.; Grätzel, M.; Gamelin, D. R. *Energy Environ. Sci.* **2011**, *4*, 1759−1764.
(25) Le Formal, F.; Tétreault, N.; Cornuz, M.; Moehl, T.; Grätzel, M.; Sivula, K. *Chem. Sci.* **2011**, *2*, 737−743.
(26) Huang, Z.; Lin, Y.; Xiang, X.; Rodriguez-Cordoba, W.; McDonald, K. J.; Hagen, K. S.; Choi, K.-S.; Brunschwig, B. S.; Musaev, D. G.; Hill, C. L.; Wang, D.; Lian, T. *Energy Environ. Sci.* **2012**, *5*, 8923−8926.
(27) Cherepy, N.; Liston, D.; Lovejoy, J.; Deng, H.; Zhang, J. *J. Phys. Chem. B* **1998**, *102*, 770−776.
(28) Pendlebury, S. R.; Cowan, A. J.; Barroso, M.; Sivula, K.; Ye, J.; Gratzel, M.; Klug, D. R.; Tang, J.; Durrant, J. R. *Energy Environ. Sci.* **2012**, *5*, 6304−6312.
(29) Cowan, A. J.; Leng, W.; Barnes, P. R. F.; Klug, D. R.; Durrant, J. R. *Phys. Chem. Chem. Phys.* **2013**, *15*, 8772−8778.
(30) Braun, A.; Sivula, K.; Bora, D. K.; Zhu, J.; Zhang, L.; Grätzel, M.; Guo, J.; Constable, E. C. *J. Phys. Chem. C* **2012**, *116*, 16870−16875.
(31) Sivula, K. *J. Phys. Chem. Lett.* **2013**, *4*, 1624−1633.
(32) Sanchez, C.; Sieber, K.; Somorjai, G. *J. Electroanal. Chem.* **1988**, *252*, 269−290.
(33) Cornuz, M.; Grätzel, M.; Sivula, K. *Chem. Vap.Deposition* **2010**, *16*, 291−295.
(34) Le Formal, F.; Gräetzel, M.; Sivula, K. *Adv. Funct. Mater.* **2010**, *20*, 1099−1107.
(35) Kennedy, J.; Frese, K. *J. Electrochem. Soc.* **1978**, *125*, 723−726.
(36) Cesar, I.; Sivula, K.; Kay, A.; Zboril, R.; Grätzel, M. *J. Phys. Chem. C* **2009**, *113*, 772−782.
(37) Dotan, H.; Sivula, K.; Grätzel, M.; Rothschild, A.; Warren, S. C. *Energy Environ. Sci.* **2011**, *4*, 958−964.
(38) Pendlebury, S. R.; Barroso, M.; Cowan, A. J.; Sivula, K.; Tang, J.; Grätzel, M.; Klug, D.; Durrant, J. R. *Chem. Commun.* **2011**, *47*, 716−718.
(39) The initial amplitude, as measured at 5 μs, is apparently maximal at 0.9 V_{RHE} before decreasing at potentials above this value. This behavior may be related to the occupancy of electronic states located at the bottom or just below the conduction and probed at 580 nm (see reference 7) that may increase or decrease the rate of "direct" recombination inside the space charge layer.
(40) The integration of the positive current does not appear to be equal to the integration of the negative current in Figure 3 (blue trace recorded at 0.8 V_{RHE}). However, at this relatively low applied potential, charge transfer to the electrolyte is not expected as this bias is below

the onset of the steady state photocurrent. We assume the discrepancy in area to be due to artefacts in the measurement of the current or to a very long recovery of the prepulse steady state.
(41) The water oxidation rate constant defined in the text corresponds to the rate constant of holes reacting with water at the semiconductor surface, as we related the initial amplitude of the second signal (long time scale) to the steady state current density extracted from the photoanode. It likely corresponds to one step of the water oxidation reaction (4-hole process), assumed to be the rate-limiting step of the reaction.
(42) Upul Wijayantha, K. G.; Saremi-Yarahmadi, S.; Peter, L. M. *Phys. Chem. Chem. Phys.* **2011**, *13*, 5264−5270.
(43) Shinar, R.; Kennedy, J. *J. Electrochem. Soc.* **1983**, *130*, 392−396.
(44) Duret, A.; Grätzel, M. *J. Phys. Chem. B* **2005**, *109*, 17184−17191.
(45) Du, C.; Yang, X.; Mayer, M. T.; Hoyt, H.; Xie, J.; McMahon, G.; Bischoping, G.; Wang, D. *Angew. Chem., Int. Ed.* **2013**, *52*, 12692−12695.
(46) Klahr, B.; Gimenez, S.; Fabregat-Santiago, F.; Bisquert, J.; Hamann, T. W. *J. Am. Chem. Soc.* **2012**, *134*, 16693−16700.
(47) Sivula, K.; Zboril, R.; Le Formal, F.; Robert, R.; Weidenkaff, A.; Tucek, J.; Frydrych, J.; Grätzel, M. *J. Am. Chem. Soc.* **2010**, *132*, 7436−7444.
(48) Sivula, K.; Le Formal, F.; Grätzel, M. *Chem. Mater.* **2009**, *21*, 2862−2867.
(49) Lin, Y.; Zhou, S.; Sheehan, S. W.; Wang, D. *J. Am. Chem. Soc.* **2011**, *133*, 2398−2401.